Transactions of the Materials Research Society of Japan 25 [2] 481-486 (2000)

Sensitive NDE of Stainless Steels by Magnetic Sensors

Koji Yamada, Katsuhiko Yamaguchi, Yosihiro Takeda, Singo Ishige, Hiroaki Kameyama, Yosihiro Isobe*

Graduate School of Saitama Univ., Urawa, Japan

Fax:+81-858-6465 e-mail: yamasan@fms.saitama-u.ac.jp

*Nuclear Fuel Ind. Ltd., Sen-nangun, Osaka 590-0481, Japan

FAX: 0724-52-7225, email: isobe@nfi.co.jp.

Nondestructive evaluations of SUS304 have been investigated by magnetic sensors of a Hall element for leakage flux observation after polarization in an uniform field, a conventional pick-up coil for magnetic noise observation to evaluate material degradation via magnetic domain wall pinning forces and by measuring magneto-resistances. Relative degradations at each position was visually demonstrated by a distribution of leakage flux gradients over structural surfaces with a high resolution of 0.3 mm in a strain range between 1 % and 8%. Internal strains can be evaluated by a magneto-resistance change for a strain range larger than 1%. The magnetization caused by martensitic transformation was estimated at about 60-80 emu/g for the fully deformed fracture state by tensile stresses up to 700MPa with the longitudinal magnetoresistance of 0.03 % in 600Oe. The total volume ratio of bcc in fcc at the fracture state is estimated at about 10% by magnetoresistance effects, in contrast to 30-40 % estimated by magnetizations.

Key words: SUS304, NDE, Hall sensor, magentoresistance

1. INTRODUCTION

Nondestructive evaluations of iron-based materials are very important because the industrial scales have grown uncontrollably large to give rise to irrevocable accidents against the safeties of civil lives. The present paper aims at the nondestructive evaluation of structural material in general industries, vessels in atomic power plants or in gas pipelines for high pressure. Among these, stainless steel is one of the most important materials and it shows magnetic property changes from a paramagnetic material to magnetic one, caused by strains inside (so called martensitic transformation). Using this phase transition, a high sensitivity inspection is possible by detecting the generated magnetism from outsides of any structures. In this paper, we aimed at the nondestructive cross evaluations of SUS304 material by using magnetic sensors of magnetism its self and by detecting resistance change in applied magnetic field (magneto-resistance effects). The magnetic tools are composed of a semiconductor Hall element for leakage flux observations in a remanent condition and a pick-up coil for magnetic noise observation. For the certainty of these evaluations, the observations were performed multiply by different tools. [1,2,3,4,5,6,7]

2. EXPERIMENTALS

The samples of SUS304 were prepared by a regular anneal after shaping samples, were applied tensile stresses and measured magnetic properties of them. The observations of other properties were carried out in cooperation with the researchers of Jpn. Soc. of Applied Electromagnetics and Mechanics (JSAEM). Each experimental procedure is as follows.

2.1 Sample preparations

SUS304 samples were prepared for round Robin tests composed of loading tests, TEM observations,

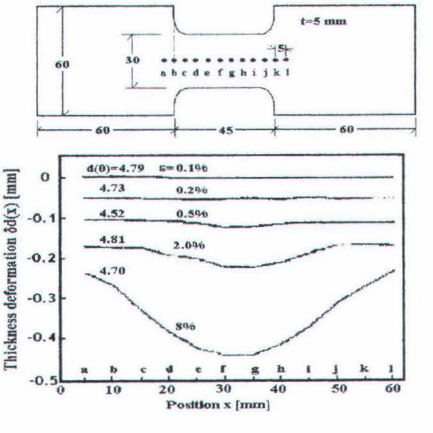

Fig. 1 Sample shape and thickness deformations with differently strains by tensile stresses up to 680 MPa

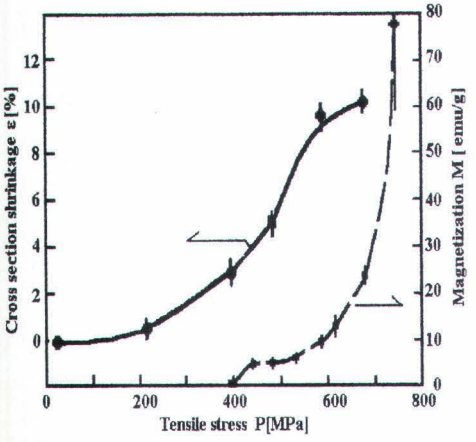

Fig. 2 The deformations and magnetizations as a function of differently strained samples.

Vickers tests, X-ray diffraction and the magnetic leakage observations [1] at each loading condition. These samples were annealed in N_2 gas at 1100 °C and were applied tensile stresses up to 690 MPa. Fig. 1 shows the sample shape and the thickness deformations along the central positions of "a" – "l". The generated magnetizations and the cross section shrinkages are shown as a function of applied tensile stresses up to fracture state in Fig. 2 . The magnetization increases rapidly just before the destruction in the fracture state in contrast to the "average" cross section change in the same range of fracture state.

2.2 Leakage flux observations

The observations of the leakage flux from the sample were performed with a semiconductor Hall sensor of GaAs mounted at the pen position of a pen-plotter instead of a pen. The leakage flux was observed simultaneously with each stage of the residual strains under loading test. The size of the Hall element has a square shape of 120μmx120μm and 50 μm thickness with a plastic cover of 100 μm. The lift-off distance was tentatively set at 200 μm from the sample surface independently of the surface roughness. Therefore, it corresponds to neglect the disturbance of the effective lift-off distance change more than 325 μm composed of the half thickness of Hall element, the apparent lift-off distance and the plastic cover. The Hall element was operated by a lock-in amplifier in a frequency of about 10 kHz and the offset Hall voltage was subtracted by a small voltage of the driving signal. 1 LSB (Least Significant Bit) corresponded to 10^{-3} Oe for 12 bits ADC by an average of 100 words, and the effective drift field of the Hall element in this total system was 0.2 Oe. The leakage fluxes from samples were observed after a uniform polarization in 1kOe along sample elongating direction Fig. 3 shows the typical leakage flux distribution of SUS304 samples. The top figure shows the sample shape as shown in Fig. 1, the second, the leakage flux gradient distribution dB_Z (x,y)/dx for a sample with ε=0.2%, illustrated in black (-) and white (+), the third for a sample of ε=2.0%, the fourth, for a sample of ε=8.0%, respectively. As apparently seen in these figures, the gradients of the leakage flux patterns are modified with the intensities of inhomogeneous local residual magnetizations (=remanence). The local magnetizations of the sample occur dominantly by the phase transition from fcc to bcc crystal transformation as mentioned before. It is worthwhile to note here that the location of the strained positions are roughly corresponds to the white spots, which will be discussed in the later sections in this paper.

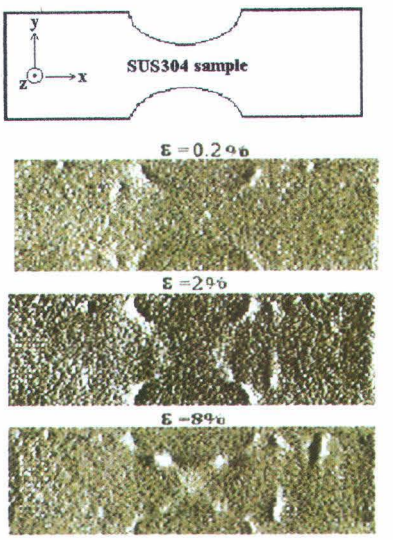

Fig. 3 The distributions of leakage flux gradients observed for SUS304 samples

2.3 Magnetic noise observations

The magnetic noise observations [8] were performed at the sample surfaces with a pick-up coil of 2 mm diameter during magnetic field sweep in a linear increasing rate as H=ct (c=2.5x10^5 A/ms) with time t. Fig.4 shows the experimental device for the magnetic noise observations. The magnetic noises were recorded by an AD converter of a resolution of 16 bits and 80,000 points at every 1μs via a CR high pass filter of 1ms time constant to eliminate the continuous part of the signal. The field sweep rate was determined to obtain the maximum information of the magnetic domain jumps in time sequences up to 70 ms as illustrated in the enlargement of Fig. 4 at which 2D fractal dimension took the maximum of about 1.66 [9]. Fig. 5 shows typical experimental results for an SUS304 samples of residual strains ranged more

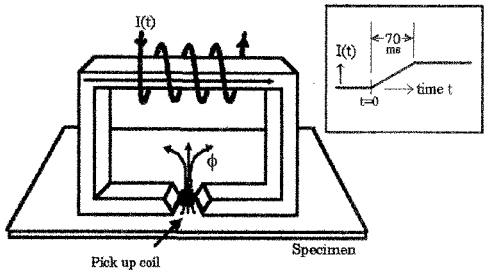

Fig. 4 The schematic view of MBN observation

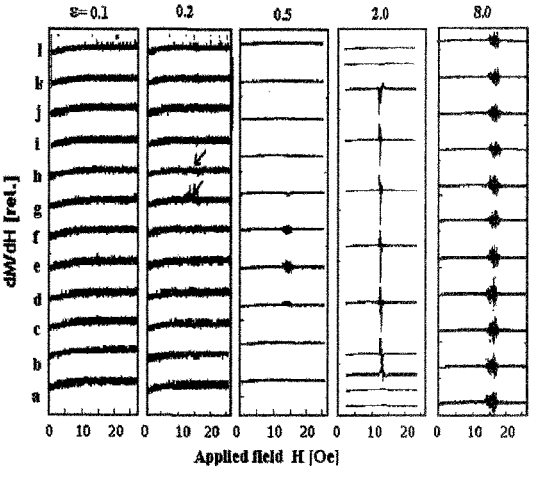

Fig. 5 Magnetic Barkhausen noises as a function of magnetic field at different position for strained samples.
[Note: magnitudes are plotted 5 times larger for the samples of ε=0.1%and 0.2 % than the others.]

than 0.1 % up to 8%. The observation points "a" to "l" are the same as in the top figure in Fig. 1. The two arrows inserted for ε=0.2% ("h" and "g" points) could be noticeable signals even for a small strains around the center of the sample. For the samples with the larger strains than ε =0.5%, the magnetic noises are really profound to be detected. These are consistent with the profiles of thickness deformations in Fig.1.

2.4 Magneto-resistance

Magneto-resistances of the stainless steel were observed by using a pulsed magnet with a long half duration of 2 sec. The configurations of magnetic fields were set in parallel (longitudinal) and perpendicular (transverse) for the sample direction. The samples thickness for this experiment was very thin as 50 μm to obtain the larger current density. The currents were supplied by a battery for the amplitude stability and the drop voltages were .measured with 16 bits ADC. The effective number must be larger than 5 decades due to the

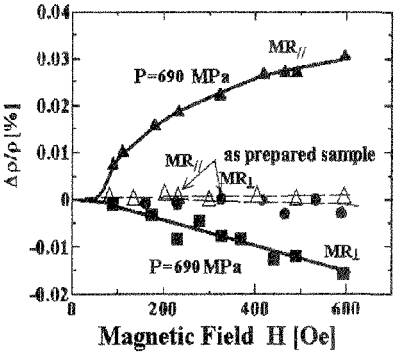

Fig. 6 MR as a function of magnetic fields.

small MR effects of about 0.1% or δR(M)/R as 10^{-4}. Fig.6 shows MR's observed in parallel configuration with x direction ($MR_{//}$) and perpendicular ($MR_{\perp}$). It must be noted here that the positive and negative MR appeared in a heavily strained sample as $MR_{//}$ and $MR_{\perp}$, which are technically convenient to make sure the signs. On the centrally to the heavily strained, MR disappeared for slightly strained samples by tensile stresses less than 400MPa.

2.5 Observation of surfaces by electron microscope

Sample surfaces were observed by an electron microscope for variously strained samples. Fig. 7 shows the photograph of the surfaces obtained by the electron microscope for as-annealed sample, and Fig. 8 for a heavily strained sample by 690 MPa. The direction of the lattice imperfection is isotropic in

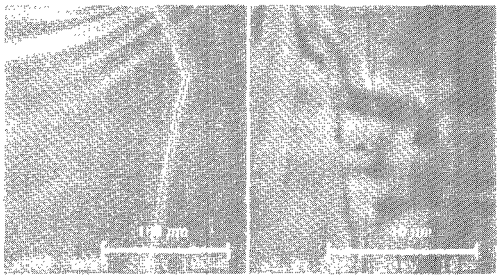

Fig. 7 The surface of an annealed sample

Fig. 8 The surface of a heavily strained sample
(The arrow shows the direction of applied stresses)

average as shown in Fig.8. The main lattice deformations show a specific direction. However, in average, the stress originated lattice imperfections seems rather irotropic for poly-crystals, which is consistent with the magnetic isotropy discussed in the next section.

4. DISCUSSIONS

In the present experiments, we observed the leakage flux distribution in the samples after polarizations in an uniform field of 1 kOe (=80kA/m), where inhomogeneous patterns appeared. There, we noticed the inhomogeneous patterns plotted by $dB_Z(x,y)/dx$ for a heavily strained sample. Further, we observed induced voltages by magnetic flux change in a pick-up coil mounted outside of the sample, which shows some relationship between the noise amplitude and the residual stresses. Therefore, we discuss now on the physical origin of the leakage flux, the amplitude of magnetic noises observed at the surface (transient leakage flux) and the optimal speed of field sweeps for magnetic noise observations. Finally we discussed about the spatial extents of the observations in this experiment.

4.1 Leakage flux

The leakage flux observation was found a visible diagnosis tool as shown in preceding sections. The leakage flux inhomogeneity of the perpendicular component (z) was given by their first derivative with respect to the position along the tensile stress. In principle, the leakage flux gradient at a position R as $dB_z(R)/dx$ is simply given by the Gauss law as follows.

$$\left[\frac{dB(R)}{dx}\right]_Z = \left[div \iiint \left\{ \frac{d\rho(r)}{dx} \cdot \frac{(r-R)}{|r-R|^3} + \rho(r) \cdot \frac{d}{dx}\left[\frac{(r-R)}{|r-R|^3}\right] \right\} dv \right]_Z \quad (1)$$

where ρ(r) denotes the local magnetic moments at each position. It is evident that the inhomogeneity of leakage flux gradient is dominantly given by the dρ(r)/dx, and little by the second term due to the small contribution in the integration of $\rho(r)d[(r-R)/|r-R|^3]/dx$. Here, the amplitude of $d\rho(r)/dx$ is determined by the inhomogeneous residual magnetization due to the locally different residual stresses caused by applied tensile stresses larger than the yield pressure. For each local magnetic moment, the remanence orientation is given by the minimum energy principle for the total magnetic energy (ε_M) composed of the anisotropy energy (ε_A) and the elastic energy (ε_E) [5, 10,11,12] as

$$\varepsilon_m = \varepsilon_A + \varepsilon_M \quad (2)$$

$$\varepsilon_A = K_1 \sum_{i \neq j} \alpha^2{}_i \alpha^2{}_j + K^2{}_2 \alpha^2{}_1 \alpha^2{}_2 \alpha^2{}_3 \quad (3)$$

$$\varepsilon_K = -\frac{3\sigma}{2} \lambda_{100} \left(\sum_i \alpha^2{}_i \gamma^2{}_i - \frac{1}{3} \right) + \lambda_{111} \sum_{i \neq j} \alpha_i \alpha_j \gamma_i \gamma_j \quad (4)$$

Here, K_1 and K_2 denote the magnetic anisotropy constants of b.c.c Fe, α_i and γ_i the direction cosine of a magnetization and a residual stress σ, respectively. λ_{100} and λ_{111} stand for magnetostrictive constants of <100> and <111> directions, respectively. Further, i and j denote the coordinates of x, y or z, respectively. The residual magnetization M_R of a sample is then given by the vector sum of the local magnetic moments as

$$M_R = \iiint \rho(r) \cos[\theta(r)] dV \quad (5)$$

Here, the microstructure of the leakage flux distribution is given only by the distribution of $\rho(r)$ as explained above. Therefore, $d\rho(r)/dx$ informs us the locally different residual stresses via leakage flux change with distances.

4.2 Magnetic noises and the optimal field sweep.

In this subsection, we examine the optimal magnetic field sweeping rate during the magnetic noise observations for the maximal information of the magnetic domain jumps in the magnetic noises. For this purposes, we calculated Fourier transforms and fractal dimensions [8] for different sample volumes of Carbonyl iron power to avoid the different anisotropic constant for different volume of small samples. The magnetic noises in powders of Carbonyl iron ranged between 0.3mg and 3.0 mg were observed and we calculated Fourier transforms and the Fractal dimensions of the original noise traces. We found a large difference among these traces. Namely, for the larger sample more than 1 mg, the continuous part of the trace become larger for which the peak position of the Fourier spectrum and it decreased with deceasing the volume. These evidences inform us that the noise observations without the considerations on the field sweeping rate is not correct. Further, the fractal dimensions of noises depended on the field sweeping speeds. It increased with decreasing field sweep speeds down to 140 kA/ms with a maximum fractal dimension of D=1.66±0.3 for 0.3mg sample. By the lower sweeping speeds than the optimum speed, signal to noise ratio (S/N) become worse, due to the smaller flux change with time. We obtained D=1.96 instead of D=2.0 for an ideal case by a simulation for the calculated white noise to make sure our calculations.

4.3 Observable spatial extent

We performed an independent experiment to prove the considerations on the spatial extent of magnetic noises and the leakage flux observations from the surface following (1)-(5). Fig. 9 shows the results of the simulation for a typical stress pattern as in Luders band [5,6].

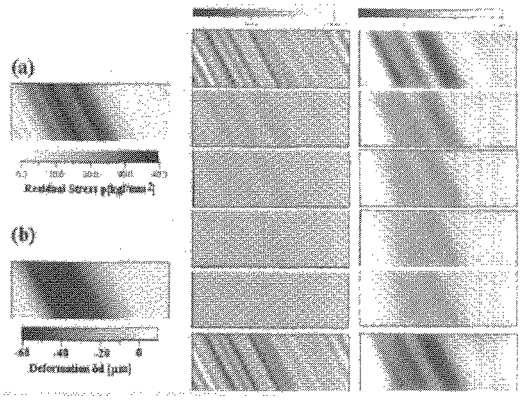

Fig. 9 Simulations of leakage fluxes
(a) Original stress pattern
(b) Thickness deformation
(c) Simulated leakage flux distribution (drown by $dB_Z(x,y)/dx$) with a lift-off distance of 0.3 mm
(d) Simulated leakage flux distribution with a lift-off distance of 3 mm.

The resolutions in this experiment is clarified by this simulations as follows [13,14]. (A) The lift-off distance dominantly determines the spatial extent of the observation as shown in Fig. 9(c), Fig.9 (d). Namely the location and geometrical extent of the inhomogeneity are discriminated by $dB_Z(x,y)/dx$. (B) The internal inhomogeneity is observable by the longer lift-off distance even with the wider resolution.

4.4 Magnetoresistance effect

We analyze MR effects to investigate on the relationship between the amplitude of MR and the volume ratio of austenite to martensite as a function of residual strain or stress. We adopt here a physical model that the austenite material has a resistivity constant $\rho_A(T, \varepsilon)$ and that martensite, $\rho_M(T, \varepsilon, M(H))$ respectively, at an ambient temperature T, residual strain ε and sample magnetization $M(H)$. For the austenite and martensite phases, the specific resistivity must be different so that $\rho_A(T, \varepsilon) \neq \rho_M(T, \varepsilon, 0)$. For the first approximation, we suppose the magneto-resistance in bcc with increasing magnetization is partly short-circuited by the remaining austenite. Therefore, the total resistivity R for the sample is expressed as

$$R_A = \frac{c\rho_A(T,\varepsilon)}{1-v} \tag{6}$$

$$R_M = \frac{c\rho_M(T,\varepsilon,M)}{v}, \quad (\rho_M = \rho_{M0} + \delta\rho_M) \tag{7}$$

Here, v denotes the volume ratio of the transformation (v=0 means whole sample is of austenite) and c, a constant. ρ_{M0} and $\delta\rho_M$ denote the resistivity of martensite in zero magnetization and the deviation from ρ_{M0} in H>0 with a condition for the real case of $\delta\rho_M/\rho_{M0} \ll 1$. The total resistance of the sample composed of R_A and R_M is approximated by their parallel connection as

$$R = \frac{c\rho_A(\rho_{M0}+\delta\rho_M)}{(\rho_A-\rho_{M0}-\delta\rho_M)v+\rho_{M0}+\delta\rho_M} \tag{8}$$

The magnetoresistance change in a field H is now expressed by the resistance $R/R(H=0)$ as

$$\frac{\delta R(H)}{R(H=0)} \approx v\frac{\delta\rho_{M(H)}}{\rho_{M0}} \tag{9}$$

Here, applied magnetic fields in an anisotropic sample must be corrected by the demagnetizing field. For this purpose, anisotropic magnetizations of the sample were measured for as-annealed and a strained sample in longitudinal and transversal directions against the sample elongating direction. Fig.10(a) shows the magnetization as a function of applied magnetic field in parallel direction ($M_{//}$) with sample elongation and that in perpendicular direction ($M_\perp$), respectively. As are easily noticed, $M_{//}$ are larger than $M_\perp$, only due to the smaller demagnetizing field caused by the anisotropic sample shape. The closed circles in this figure, denote $M_\perp(H^*)$ in effective fields $H^*=0.33H$, where evidently $M_\perp(H^*)$ well coincides with $M_{//}(H)$. Fig.10(b) shows longitudinal and transversal magnetizations of a strained sample. Closed circles denote $M_{//}(H^*)$ as a function of applied field H where closed circles coincide well with $M_{//}(H)$. Fig.10(c) shows $\delta R_{//}(H^*)/R_{//}(0)$ and $\delta R_\perp(H^*)/R_\perp(0)$ as a function of H^* for differently strained samples. As is easily noticed, the magnitude of negative MR is almost equal to that in positive longitudinal MR. The origins of MR for iron or Ni had been discussed in ref.[15,16].

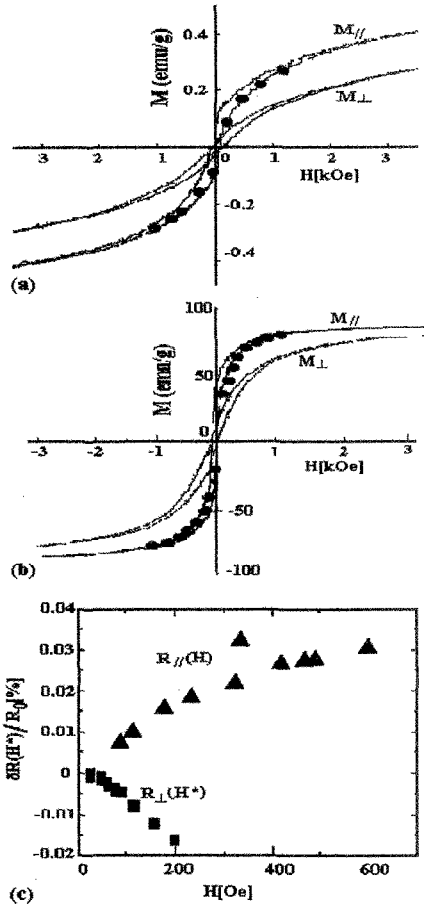

Fig. 10 The magnetization and MR for an annealed sample and a heavily strained sample.

(a) Original M-H curve (solid lines) and corrected M-H curve (solid circles) by demagnetizing field for an annealed sample.

(b) Original M-H curve (solid lines) and corrected M-H curve (solid circles) by demagnetizing field for a heavily strained sample

(c) MR for a heavily strained sample corrected by demagnetizing field.

It is apparent that the magnitudes of longitudinal MR shows almost isotropic if we adopt the effective field in Fig.10(a) and Fig.10(b). These are consistent with the observations of the surface state as shown in Fig.8 (right figure) for polycrystalline SUS304 material. Further, the magnitudes of longitudinal MR are determined by magnetizations of the sample, which are very abruptly increase in a fracture range as shown in Fig. 2. Therefore, it is very easy to find the degradation by this method. Finally, the volume ratio of the bcc in fcc must be discussed here. The magnitude of MR is limited less than 0.03 % for heavily strained sample more than 10%, in comparison with 0.3% [14] for pure iron. Therefore, the volume ratio must be 10 times smaller than that compared with the magnetization of 40 % (80 emu/g) as shown in Fig. 2. It is worth while to note that the magnetization of the sample could not be the index of the real volume ratio of bcc in fcc in SUS304.

4. CONCLUSIONS

In the presented paper, we showed the fractal dimensions of the original magnetic noise traces were maximized to obtain the full information of the magnetic domain de-pinning with a proper field sweeping speed. The extent of the observation range with the present method was found within about 50 μm proved for a stretched pipe line of iron based material. The maximum volume ratio of bcc in fcc induced by martensitic transformation is estimated about 10% by MR effects, rather than 40 % estimated by magnetizations.

Acknowlegdement

Authors thank to Prof. Uesaka, Univ. Tokyo for his helpful discussions

REFERENCES

[1]M. Uesaka et al. Proc. Int Workshop on Electromagnetic N.D.E, Reggio Calabria, Italy(1997)

[2]K. Yamada et. al., Proc. Int. Workshop on Advanced Mechanics (IWAM '97), Nagasaki,114-119 (1997)

[3]K.Yamada et al. Proc. Int Symp. on Electromagnetism (ISEM '97), Germany, June,153-156 (1997)

[4] K. Yamada, S. Shoji, Y. Tanaka, Y. Uno, H. Takeda, S. Toyooka, Suprapedi, Y. Isobe, K.Ara, M. Uesaka and K. Miya, J. Magn. Soc. Jpn, 23, 718-720 (1999)

[5] S. Shoji, Doctor Thesis, Mar. (1999) Saitama Univ.

[6] Suprapedi et.al. Opt..rev., 14, No2, 284-287 (1997)

[7]K. Yamada et.al., Proc. Int. Conf. Advanced Mechtronics, (IWAM'99, Chunchon, Korea), Invited paper, 1-6 (1999)

[8]D.C. Jiles, Review of magnetic method for nondestructive evaluation,NDT Int., 21,311-319(1988)

[9]K. Yamada et.al. J. Mag. Magn. Mater. 104-107,341-342(1992)

[10]G. Rieder, Abhandl. Braunchweig. Wiss. Ges., 11,20 (1959)

[11]J.Weertman and J. R. Weertman, Physcalmetallurgy, Third and enlarged Ed., Ed. R.W.Chan, P. Haasen, Elsevier Sci., Publ. Amsterdam, 1282 (1982)

[12] K. Yamada, P. Lim, S. Shoji,H. Takeda, S. Toyooka, Sprapedi, T. Masuda and N. Hagiwara, Proc. 32nd ISATA, Material for Energy Efficient Vehicles, Vienna, June, 573-580 (1999)

[13] K. Yamada, S. Shoji, Y. Isobe, M. Uesaka and K. Miya, Proc. 7th Int. Conf. Nucl. Eng., Tokyo, April (1999) ICONE, CD Publ (ICONE-7054).

[14]K. Yamada et.al., Special Issue of Int. J. Appl Eelctromagnetism and Mech., to be printed.

[15]R. Bekker u et al. Ferromagnetism (Springer , Berlin)469 (1939)

[16] E. Englett, Ann. Physik, 14,469 (1932).

(Received January 24, 1999; accepted January 31, 2000)